ORIGINAL ARTICLE

Fracture characteristics of Hongcheon Gneiss in South Korea assessed from deep drillcore samples

Youjin Jeong[1] · Jaeho Lee[1] · Junghae Choi[2] · Dae-Sung Cheon[3] · Byung-Gon Chae[3]

Abstract

Fractures in a rock mass have an important influence on the mechanical response and hydraulic properties. Investigating and modeling fractures is crucial, especially with regard to the geological disposal of high-level radioactive waste, where long term stability is necessary to avoid a direct threat to society. This study sought to classify joints and faults in the Hongcheon gneiss, South Korea, based on their geometric characteristics. A generic classification model for joints and faults is proposed, dividing them into four types based on propagation pattern and development of fault core and fault effect zone. More than 4,000 joints and 34 faults were analyzed using samples of deep drillcore to investigate the relationships between the properties of these structures and depth or lithology. To validate the model, it was applied to other area where different lithologies are found. A damage index is utillized to visually represent the impact of a fault on the quality of rock mass. The joint patterns can be correlated with lithology, as the mineralogical characteristics and internal structures influence the patterns. The fault zone patterns show a relationship with depth, and the damage index provides a reliable indication of the fault impact. The validation of the fault model will be conducted in subsequent studies. With estimation of the hydromechanical properties of each joint and fault pattern, a practical approach would be provided to characterize fractures from drillcore data and enhance the accuracy of fluid flow and stability models for any given rock mass.

Keywords Joint · Fault · Fluid flow · Geological disposal · Site characterization

Introduction

Analyses of fractured rock masses, which represent a ubiquitous geomaterial, are necessary to address the urgent worldwide need for the disposal of high-level radioactive waste (HLW). The aim of HLW disposal is to isolate radionuclides and prevent their migration until decay. Meeting this need requires an understanding of rock mass fracture systems, which play a crucial role in determining the hydromechanical behavior of rock.

In this paper, the term 'fracture' is used as a general term encompassing any mechanical break that separates a rock mass into two or more parts, including joints and faults (Gudmundsson 2011). The term 'fault' refers to a fracture with observed displacement and/or fault surface structures (Petit 1987). The term 'joint' refers to a natural fracture with opening displacement (Pollard and Aydin 1988).

Fractures affect the properties of rock (Bandis et al. 1983; Barton 1972, 1973, 1974, 1976; Barton and Choubey 1977; Jaeger 1959; Patton 1966), the deformation and failure of rock (Jiang et al. 2014; Kim et al. 2012; Li et al. 2014), and groundwater flow and solute migration (Bodin et al. 2003; Boutt et al. 2006; Zimmerman and Bodvarsson 1996). Particularly in the case of HLW disposal, fractures are the primary research targets because they serve as potential flow paths that offer the minimum resistance to fluid flow. Lofi et al. (2012) proposed using fluid circulation and optical and acoustical images to observe discontinuities and estimate their potential transmissivity. De Vargas et al. (2022) investigated groundwater flow in fractured rock masses and found that the presence of fractures creates preferential

✉ Junghae Choi
choi.jh@knu.ac.kr

[1] Department of Geology, Kyungpook National University, Daegu 41566, Korea

[2] Department of Earth Science Education, Kyungpook National University, Daegu 41566, Korea

[3] Geology and Space Research Division, Korea Institute of Geoscience and Mineral Resources (KIGAM), Daejeon 34132, Korea

pathways, significantly affecting the groundwater flow pattern and circulation.

Among the properties of joints, the surface roughness has a strong influence on shear behavior, strength, deformability, permeability, and flow properties (Kulatilake et al. 2006; Ye and Ghassemi 2018; Ye et al. 2018a, b). The joint surface roughness can significantly influence flow field complexity and can cause nonlinear flow behavior (Cardenas et al. 2007; Lee et al. 2014, 2015; Pirzada et al. 2022; Zimmerman et al. 2004; Zou et al. 2015). Thus, quantifying joint roughness is needed to model the hydromechanical behavior of rock joints.

The many methods developed to quantify joint roughness can be classified into contact and non-contact approaches. Contact methods are employed in practice because of their low cost, but they are relatively labor intensive because they require physical contact with joint surface. Representative examples of contact methods include the linear profiling method (Barton 1978; Keller and Bonner 1985; Schmittbuhl et al. 1995), the compass and disc clinometer method (Fecker and Rengers 1971), the shadow profilometry method (Maerz et al. 1990), the tangent plane sampling and pin sampling method (Rasouli and Harrison 2000), and the mechanical or electronic stylus profilometry method (Aydan et al. 1996; Brown and Scholz 1985; Develi et al. 2001; Du et al. 2009). In contrast, non-contact methods have become more widely used because they can provide high-resolution data and are less time-consuming, thanks to technical advances. These methods include laser scanning (Fardin et al. 2001, 2004; Feng et al. 2003; Ge et al. 2014; Zheng et al. 2021), laser profilometry (Brown 1995; Hsiung et al. 1993; Jiang et al. 2006; Kulatilake et al. 2006), stereo-topometric cameras (Grasselli et al. 2002; Hong et al. 2008) d ray computed tomography (Johns et al. 1993). In addition to these methods, empirical methods are typically used (Barton 1982; Barton and Choubey 1977). Given the highly erratic nature of joint surface topography, statistical parameters are used to represent joint surface roughness (Tatone and Grasselli 2010; Zhang et al. 2014). Methods based on fractal characteristics are also employed (Babanouri et al. 2013; Kulatilake et al. 2006; Lee et al. 1990; Li and Huang 2015; Shirono and Kulatilake 1997).

The most widely used parameter in quantifying joint surface roughness is the joint roughness coefficient (JRC), which was initially proposed by (Barton 1973) and later adopted by the International Society for Rock Mechanics (Barton 1978). JRC describes the geometry of a surface in terms of waviness and unevenness. Both terms refer to scale, so that waviness refers to a dominant larger scale, while unevenness refers to a small scale that is randomly distributed. Although the concise form and simple application of JRC have attracted many users, this approach has shortcomings (Kodikara and Johnston 1994; Kulatilake et al. 1995; Maerz et al. 1990).

Faults can act as fluid flow conduits and provide the means of flow entry and exit (Aydin 2000; Caine et al. 1996; Martin et al. 2005). In general, bulk rock permeability is higher near a fault zone than in the protolith, due to an increase in fracture density and connectivity. There have been many studies by structural geologists and hydrogeologists aimed at evaluating the influence of faults on fluid flow and examining their architecture, and the approaches and methods taken have been quite varied according to the particular field of study. Bense et al. (2013) demonstrated a holistic understanding of fault zone hydrogeology from among these multiple disciplines. Surface-focused studies by structural geologists have led to investigations of fault zones in various geological settings, and Caine et al. (1996) proposed a fault zone architecture and permeability structure that is widely used. In the subsurface-focused studies of hydrogeologists, boreholes have been used to investigate the hydrogeological behavior of fault zones, typically without direct observation of outcrops. Various methods have been developed to enhance the performance of flow simulators or models. Flodin et al. (2001) developed and applied a procedure for assigning permeability values to each grid block representing the fault zone in a flow simulation model. They assigned permeability values based on the thickness and permeability of the fault zone. Islam and Manzocchi (2019) developed a flow-based geometrical upscaling method to capture the effects of three-dimensional fault zone structures in conventional low-resolution upscaled flow simulation models. Liu et al. (2019) modeled branched and intersecting faults using the extended finite element method and developed a new enrichment strategy. All these researchers reported that specifying and quantifying values for a fault zone is necessary but challenging, given the highly complex structure, heterogeneity, and anisotropy of faults.

As stated above, fractures have a significant impact on the behavior and frequent anisotropy of rock masses (Barton and Quadros 2015). Recent studies have shown more sophisticated methods to simulate fractured rock masses using advanced computing technologies, such as extended finite element method (Deb and Das 2010), 3D finite difference method (Sun and Yang 2019), 3D discrete element method (Scholtès and Donzé 2012), statistical damage constitutive model (Wu et al. 2022), CNN-based constitutive model (Wu et al. 2023).

Nevertheless, accurately predicting the behavior of rock masses remains challenging due to its inherent heterogeneity. Furthermore, despite the numerous studies that have characterized joints and faults, it is difficult to apply the proposed methods to drillcores. There have been few attempts to measure the JRC of subsurface joints, as it is time- and

energy-consuming to observe the surfaces of joints in drillcore. In addition, the widely used model of fault zone architecture is not adequate for drillcore studies due to the differences in scale. Therefore, in this paper a generic classification model for joints and faults is proposed to overcome the limitations of current methods when analyzing deep borehole data. The criteria were set by simplifying the geometries of joints and faults in the Hongcheon area, South Korea. The distributions of the classified groups and the relationships between the distribution and depth were analyzed. The distribution of lithology for each joint type was also investigated to understand the influence of mineralogical characteristics on joint type. The damage index was used to graphically indicate the impacts of faults on the quality of rock mass. Finally, the validity of the model was tested by applying it to another area with different lithologies.
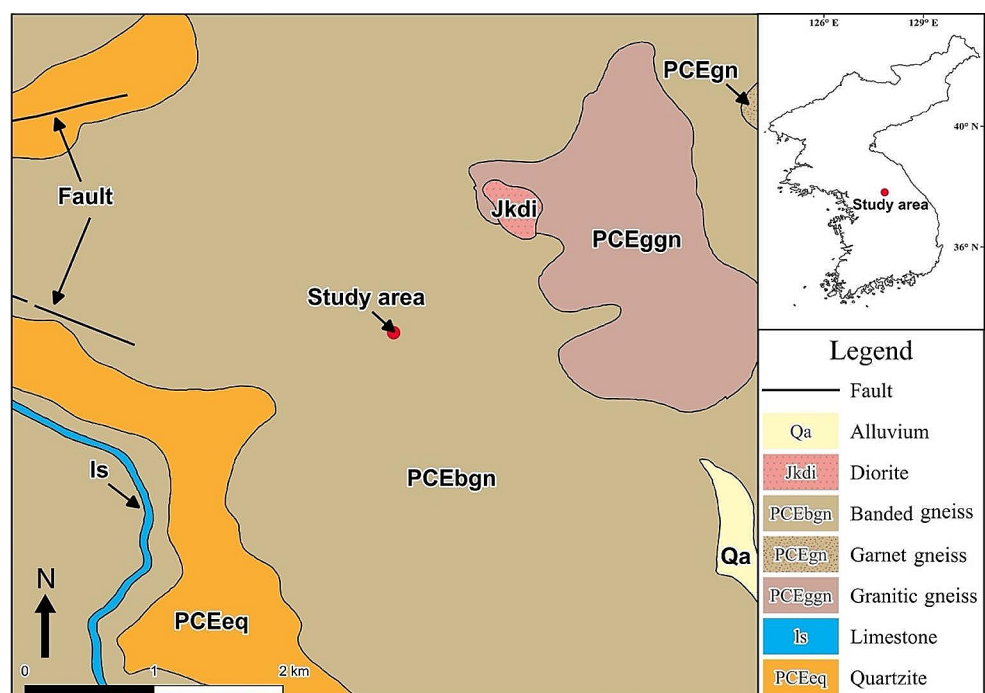
Materials and methods

Materials

Hongcheon is located in the northeastern part of the Gyeonggi Massif where the Yongduri gneiss suite is exposed. Figure 1 shows a geological map of the study area (Son et al. 1975). The area is dominated by biotite gneiss, including porphyroblastic gneiss, banded gneiss, and augen gneiss, along with non-gneissic lithologies such as pegmatite. Several faults have been identified in the study area.

To obtain data on rock masses at depth, a vertical hole was drilled (SP 5500SA with NQ3K) to a depth of 761.6 m.

A triple core barrel was applied, and drillcore was recovered by raising the inner tube using a wire rope. To increase the core recovery ratio, the core recovery interval was reduced from 3 m to < 1 m when the rock quality was low. The recovered drillcores are typically dark or light gray in color.

Methods

The field investigation was focused solely on natural fractures, and it excluded drilling-induced fractures. The depth of fractures was measured using the scanline method. To address the problem of core loss in the fracture zone, the width of the fracture zone and the sizes of grains within the fracture zone were analyzed to obtain the modal grain size. In the case of missing data within the fracture zone, the modal grain size was used. In the study area, joints and fault zones have four main geometrical characteristics.

There are two conceptual models for joints (Du et al. 2014; Yoshida et al. 1989) that share the same criteria and conceptual groups. Figure 2 shows the classification process and examples of joint patterns. Joints were primarily characterized according to whether a change in propagation direction was observed on the drillcore surface. If the direction of propagation remained constant (i.e., within ~30°), the propagation path was classified as a planar (P) type if roughness was low and as an irregular (I) type if roughness was high. If the propagation direction changed by $\geq 30°$, the joint was categorized as a curved (C) type if the perpendicularity of inflection point was low, and as a stepped (S) type if the perpendicularity of inflection point was high. Here, these patterns are termed 'joint patterns'.

Fig. 1 Geological map showing the location of the Hongcheon area

Fig. 2 Classification of joints and representative joint patterns; Retrieved from Du et al. 2014; Yoshida et al. 1989

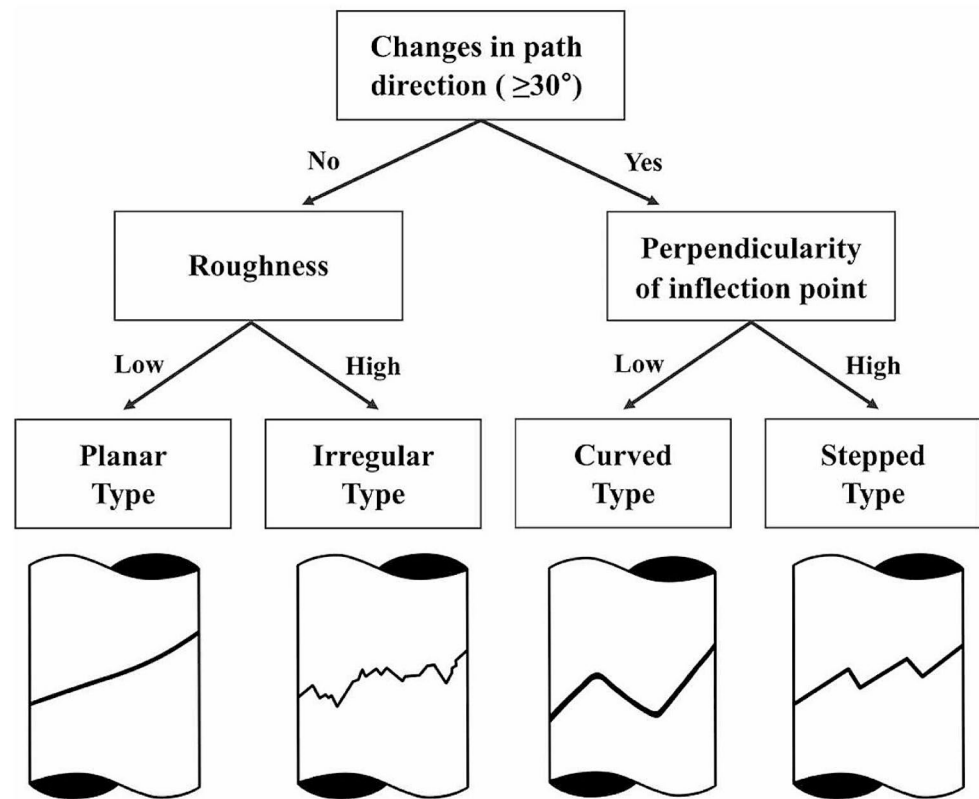**Table 1** Distribution of lithologies in the Hongcheon area

Lithology		Total Thickness (m)	Proportion (%)
Group	Lithology		
Gneissic group	Augen gneiss	83.30	11.0
	Banded gneiss	88.65	11.8
	Biotite gneiss	298.20	39.5
	Chlorite gneiss	25.80	3.4
	Garnet gneiss	40.80	5.4
	Leucocratic gneiss	5.65	0.7
	Porphyroblastic gneiss	129.05	17.1
Non-gneissic group	Pegmatite	32.45	4.3
	Quartzite	0.30	0.1
	Migmatite	1.20	0.2
	Mylonite	49.05	6.5

Joint patterns are influenced by factors such as stress conditions, rock structure, and mineral composition. Since it is challenging to determine the stress conditions at depth, the distribution of joint patterns with depth was analyzed, interpreting increasing depth as representing increasing stress. The ways in which joint pattern distributions differ at depths of 0–250, 250–500, and 500–761.6 m were examined. To identify the influence of mineral composition on joint patterns, the variations in the distributions of lithologies relative to each joint pattern were investigated by specifying 11 lithologies: augen gneiss, banded gneiss, biotite gneiss, chlorite gneiss, garnet gneiss, leucocratic gneiss, porphyroblastic gneiss, pegmatite, quartzite, migmatite, and mylonite (Table 1).

For the 34 fault zones identified in the study area (Table 2), their geometries can be described in terms of two main elements, the core and fault effect zones, and each of these zones can be further divided into two types. Thus, the geometry of fault zones in the Hongcheon area can be categorized into four types according to the degree of development of the core and fault effect zones, as shown in Fig. 3a. Type 1 is a single fault plane that is not accompanied by a network of fractures and has the least-developed core and fault effect zone. Type 3 is a single fault plane with gouge, and it is a combination of the least-developed fault effect zone with a more-developed core than type 1. Type 2 has a higher degree of fault core and fault effect zone development with grain size reduction observed toward the fault core. Type 4 is a combination of low fault core development and high fault effect zone development where the fault gouge and breccia appear to have been lithified. The four types with descriptions are shown in Fig. 3b.

Faults have different geometries according to their stage of evolution and their influence on adjacent fractures. Peacock (2001) reported that joints may exist before faulting but that faulting also leads to the initiation of new joints. Joints initiated by a fault behave differently from those that

Table 2 List of fault zones in the drillcore

No.	Depth (m)		No.	Depth (m)	
	Start	End		Start	End
1	17.10	17.40	18	263.30	263.40
2	34.30	34.40	19	420.92	
3	104.95	105.30	20	447.32	447.34
4	105.30	105.50	21	455.30	455.50
5	122.10		22	489.25	489.40
6	135.21	135.30	23	504.32	
7	135.60	135.80	24	505.45	505.51
8	139.90	140.10	25	505.90	506.20
9	163.60	163.65	26	621.80	622.10
10	174.40	174.50	27	624.09	
11	176.10	176.75	28	624.60	
12	177.28	178.26	29	633.70	633.80
13	250.47	250.50	30	634.20	634.32
14	250.68	250.70	31	703.66	703.80
15	251.40	251.41	32	741.30	741.60
16	251.68	251.78	33	749.60	
17	253.36	253.40	34	751.87	

existed before faulting. The energy released by faulting determines the type and range of fault impacts. However, it is challenging to assess the energy and damage zone of faults with drillcores because of limited observation. Therefore, the spatial arrangements of fractures near fault cores were analyzed to estimate the energy of faulting. To calculate the degree of fracturing, the number of fractures was counted toward the surface and downward, and the distances of the 10th, 15th, and 20th fractures from the fault core were calculated by using $Dist_i = |Depth_i - Depth_{core}|$, where i is 10, 15, or 20; $Depth_i$ refers to the depth of the ith fracture; and $Depth_{core}$ refers to the depth of the fault core. The calculated distances were averaged for the depth ranges of 0–250, 250–500, and 500–761.6 m to assess the relationship between depth and distance of fractures from the fault.

Menéndez et al. (1996) proposed the damage index to quantify the extent of damage in relation to mineralogy. Initially, it was employed to indicate the extent of microcracking, although it continues to possess utility in the context of drilling cores. To depict the impact of faults visually, criteria of damage index was developed by modifying the rock mass rating (Bieniawski 1974). The damage index showcases the degree of fracturing determined by the average spacing within a unit range, as shown in Table 3. The unit range was established as 2.8 m, considering the distances of the 10th, 15th, and 20th fractures in the fault core. This approach offers the advantage of providing a concise overview of the degree of crushing near the fault and its variation with depth.

Results

Joint pattern distribution

Figure 4 shows the proportion of each joint pattern, with the most abundant being the I type, followed by the S, P, and C types. Figure 5 shows the relationship between joint pattern and depth. The I type generally increases in abundance with depth, whereas the P, S, and C types generally decrease. The I type is the dominant type at all depths, accounting for 87.5%, 89.6%, and 92.4% of all joints at depths of 0–250, 250–500, and 500–761.6 m, respectively. The trends with depth differed among the other types, with the abundance of S type decreasing from 6.4 to 4.7% with increasing depth, and the abundance of P type decreasing from 5.8 to 2.8%. The C type is most abundant at 0–250 m depth, but is < 1% at all depths.

An analysis of the distribution of lithologies was conducted for each joint pattern, classifying lithologies into gneissic and non-gneissic groups (Fig. 6). The C type had a higher abundance in the non-gneissic group. The other three types generally have similar abundances in both groups of lithology, but the I type had a high abundance in the porphyroblastic gneiss.

Figure 7 shows representative examples of each fracture pattern in drillcore. The P type is characterized by a straight, knife-like line, while the I type is more jagged. The S type shows a continuous change in the path of the fracture compared with P and I types, and the C type shows a smooth inflection point with a change in path, unlike the S type. Using these patterns, it was possible to distinguish 4,025 joints with the naked eye.

Characterization of fault zones

Figure 8 shows the result of classifying all fault zones in the study area using the generic model. Type 2 is the dominant fault zone type, followed by types 1, 3, and 4. Figure 9 shows the proportions of fault core types at depths of 0–250, 250–500, and 500–761.6 m. Types 1 and 3 show an increase in abundance with depth, while types 2 and 4 show a decrease. In particular, type 1 shows an increase from 7.7 to 41.7% with depth, whereas type 3 increased by 11.7%. Type 2 decreased by 32.2%, while type 4 is absent at depths of 500–761.6 m.

Figure 10 shows representative examples of each fault zone pattern in drillcore. Type 1 is characterized by a single fault plane that is not accompanied by a network of fractures and has the least-developed fault core and effect zone. Type 2 shows a higher degree of fault core and effect zone development with grain size reduction toward the fault core. Type 3 is characterized by a single fault plane accompanied by

Fig. 3 The criteria for classifying a fault zone (**a**) and the four representative types with descriptions (**b**)
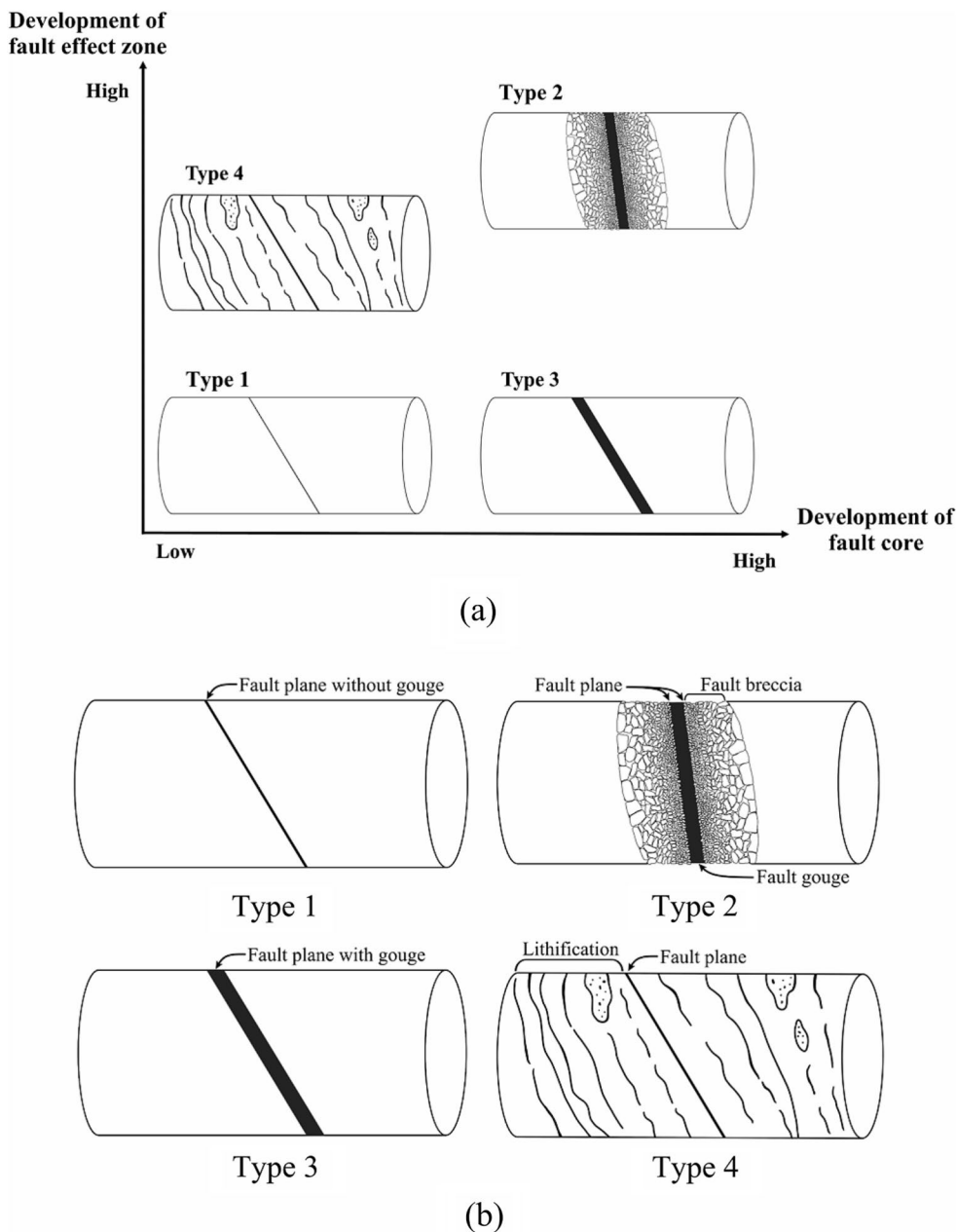

(a)

(b)

Table 3 Criteria used to calculate the damage index

Index	0	1	2	3	4
Number of discontinuities (x)	$x = 0$	$1 \leq x < 2$	$2 \leq x < 8$	$8 \leq x < 21$	$21 \leq x$
Average spacing (m)	<0.40	0.20–0.40	0.06–0.20	0.02–0.06	<0.02
Description	Intact	Slightly fractured	Fractured	Highly fractured	Severely fractured

fault gouge with the least-developed effect zone and a more-developed core than Type 1. Type 4 shows a combination of low fault core development and high effect zone development where the fault gouge and breccia appear to have been

lithified. The 34 fault zones were distinguished using these fault zone patterns with the naked eye.

The spatial arrangement of fractures near fault zones was analyzed to conduct a quantitative assessment of the impact of faults on the quality of rock mass (Fig. 11). In both directions, toward the surface and downward, the distances of the 10th, 15th, and 20th fractures from the fault core increase with depth. In particular, the directions toward the surface show a greater variation with depth than those in the downward direction. The maximum average distance was 2.8 m.

To depict visually the impact of a fault, a damage index was assigned to each unit range (0.4 m) within the total range of 2.8 m around each fault (Table 3). The determination of
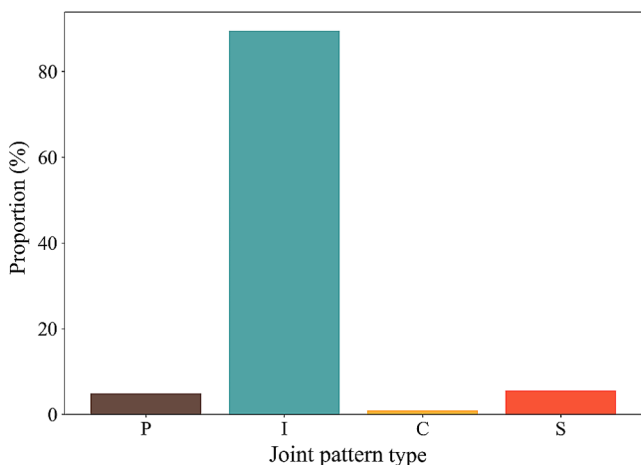
Fig. 4 Proportions of the four joint pattern types (total: 4,075)

the total range was based on the maximum average distance
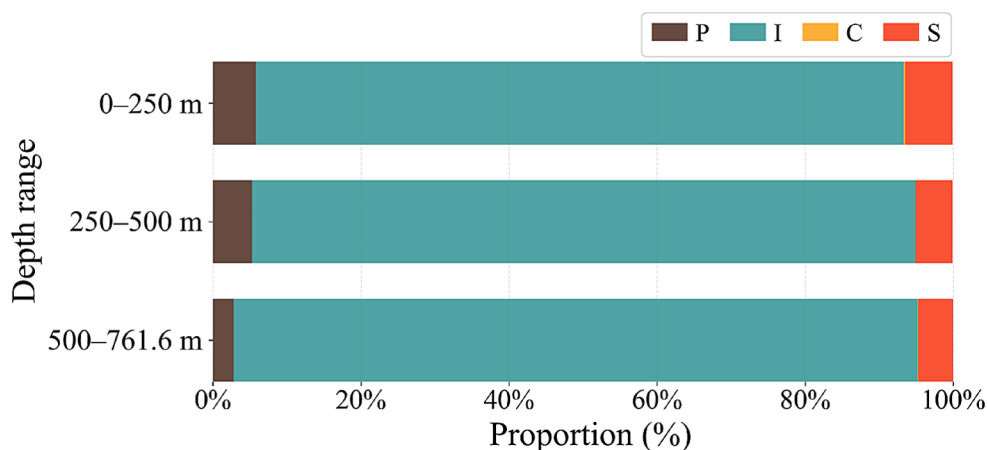
from fault core toward both the surface and greater depths. Figure 12 shows a damage index map for faults in the study area. The results show an increasing proportion of damage index values of 0 and 1 with increasing depth, indicating a higher quality of rock mass with increasing depth.

Validation

To validate the proposed model, it was applied to a region with different lithologies with the same method. The Yeongam area is on the southwestern coast of the Korean Peninsula, where extensive land reclamation has occurred and only a few natural features are observed. Figure 13 shows the lithologies in the area. The representative lithologies can be categorized broadly as bedrock, Paleoproterozoic granites and schists of unknown age, Mesozoic intrusive rocks, and various Cretaceous tuffs that unconformably overlie the

Fig. 5 Proportions of joint patterns at different depths

Fig. 6 Proportions of joint patterns at different depths

(a) P type

(b) I type

(c) C type

(d) S type

Gneiss group
Augen gneiss
Banded gneiss
Biotite gneiss
Chlorite gneiss
Garnet gneiss
Leucocratic gneiss
Porphyroblastic gneiss

Non-gneiss group
Migmatite
Mylonite
Pegmatite
Quartzite

Fig. 7 Photographs of examples of each joint pattern; (**a**) Planar type, (**b**) Irregular type, (**c**) Curved type, (**d**) Stepped type
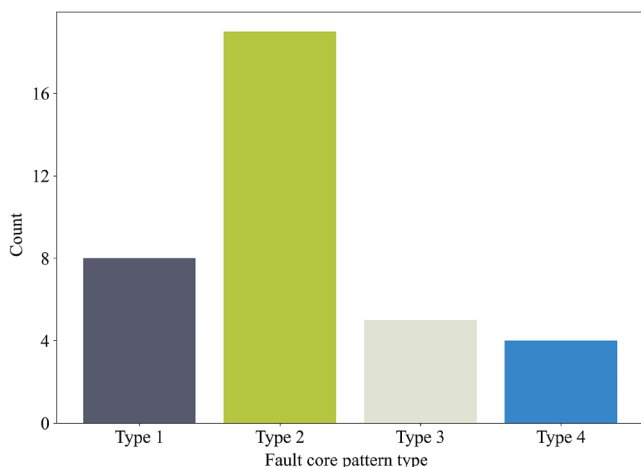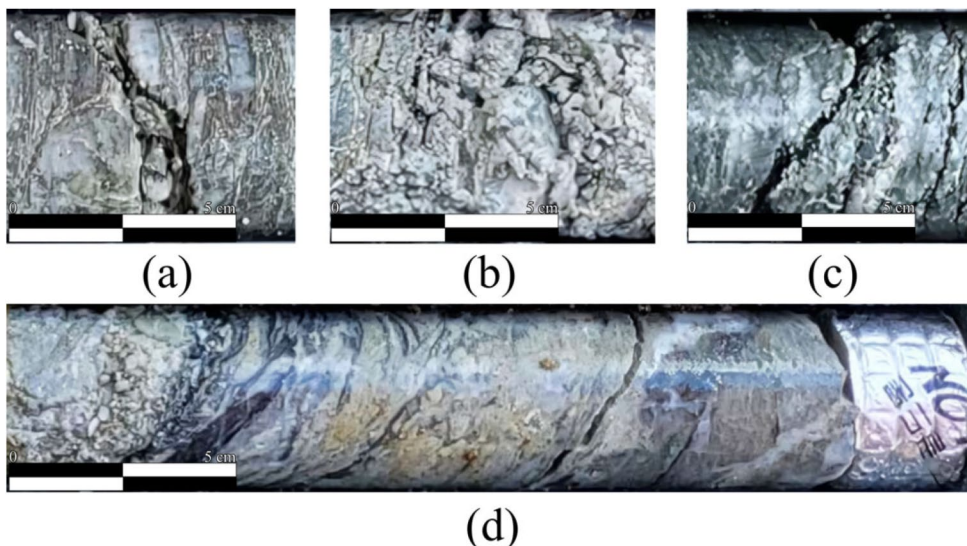

Fig. 8 Counts of fault zone patterns in the study area

numerous clasts. The sporadically distributed tuffs contain centimeter-sized volcanic clasts in a tuffaceous substrate, and show sedimentary-like bedding.

As a result of obtaining information about the rock types and discontinuities in the area from drillcores obtained by the same type of drilling as in the Hongcheon area, 2509 fractures were identified, and all fractures could be classified using the joint model. The joints were divided into pattern types, with the order of abundance of types (from high to low) being I, P, C, and S (Fig. 14). As in the Hongcheon area, the I type was most dominant, but the P type is more abundant (35%) in Yeongam than at Hongcheon. In terms of the proportion of types with depth (Fig. 15), the P type is more abundant (>40%) in the upper part of the profile and makes up ~20% at depths of 250–500 and 500–750 m, while the I type is most abundant (49.4%) in the upper part and makes up ~60% of joints in the 250–500 and 500–750 m depth ranges. The C type is least abundant in the upper part and increases in abundance with depth, while the S type makes up ~1% of the total joints at all depths.

other rocks. The lithologies observed in drillcore are mostly Cretaceous rhyolite and tuff, and the variation of rock types is relatively less than that in the Hongcheon area. The rhyolite is milky white or greenish gray in color and contains

Fig. 9 Proportions of fault zone pattern types at different depths
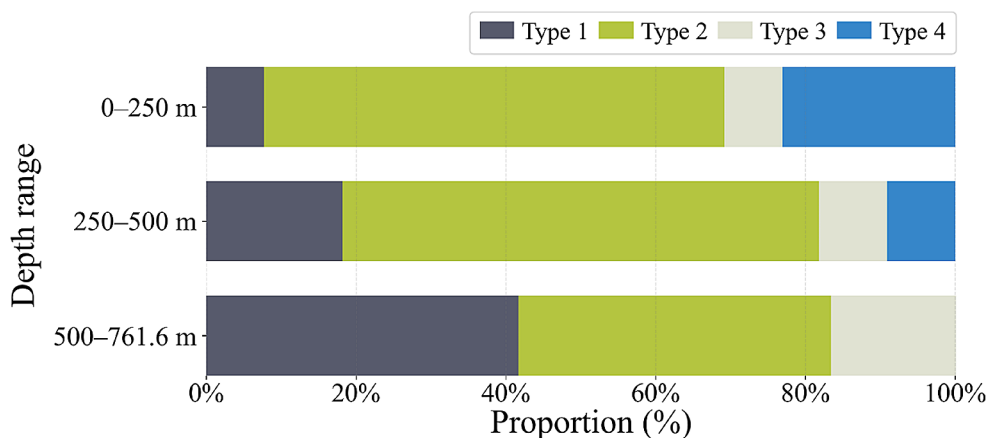
Fig. 10 Photographs of examples of each fault zone pattern
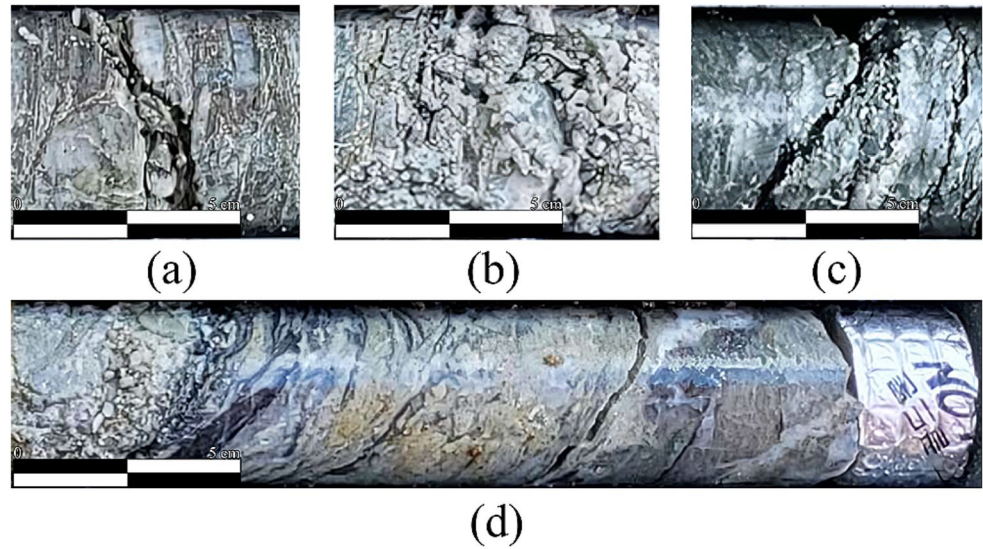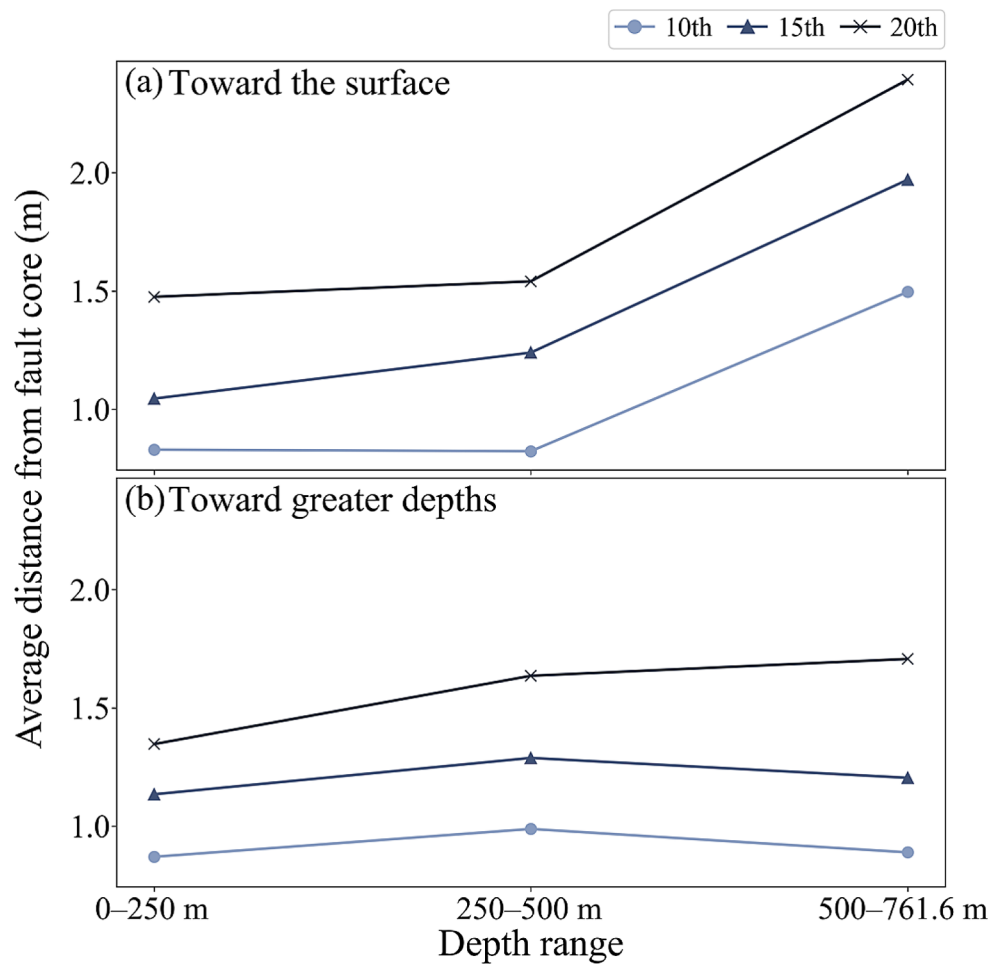

(a) (b) (c)

(d)

Fig. 11 Average distances from the fault core of the 10th, 15th, and 20th discontinuities, toward the surface and toward greater depths


Validation of the fault model in the Yeongam area was not possible because only a few fault zones were found. Further studies may validate the fault model when drillcore data from other faulted areas become available.

Discussion

The aim of the joint pattern model is to provide an effective representation of hydraulic conductivity. Although the significance of joint roughness in hydraulic conductivity is

Fig. 12 Damage index values for fault zones in the study area
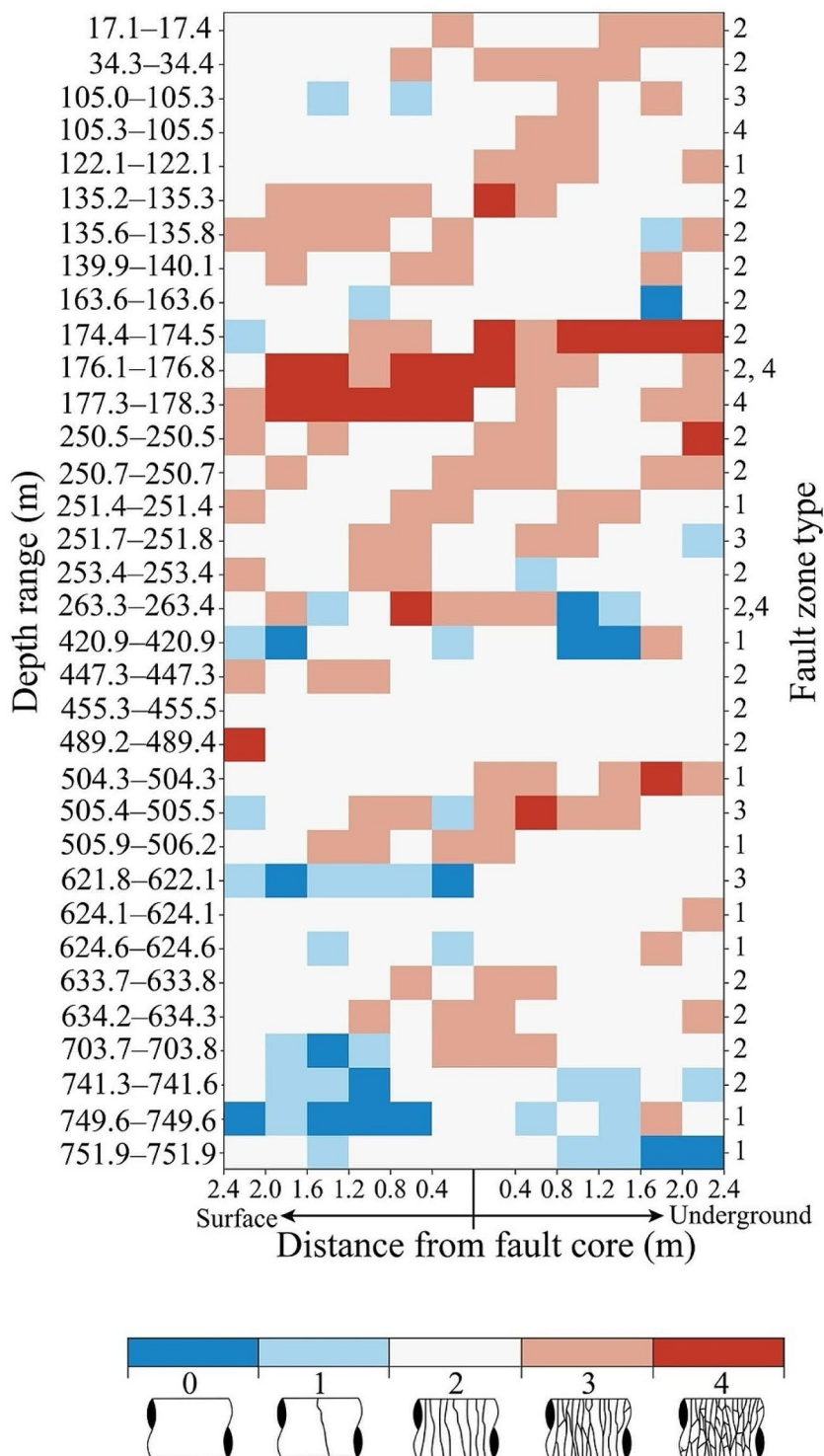
well recognized, it can be neglected in practice because of challenges in expressing joint roughness in hydraulic terms. In the proposed model, the P type could be deemed to have a lower joint roughness than the other types. Considering that fractures with low surface roughness develop preferential flow (Scesi and Gattinoni 2007), the P type is inferred to be the most favorable joint type for fluid flow.

Joint patterns of the P, I, and S types are consistently more abundant within the gneiss group than the C type, and they generally show similar proportions of lithologies (Fig. 6). Notably, there is a relatively high number of I and C types in the porphyroblastic gneiss and the non-gneissic group, respectively. Fractures in rock masses can be categorized into four groups: intragranular, intergranular, transgranular,

Fig. 13 Geological map of the Yeongam area, showing the location of the study area
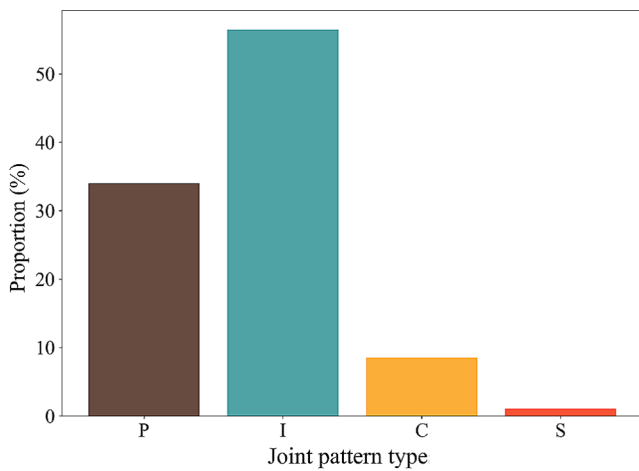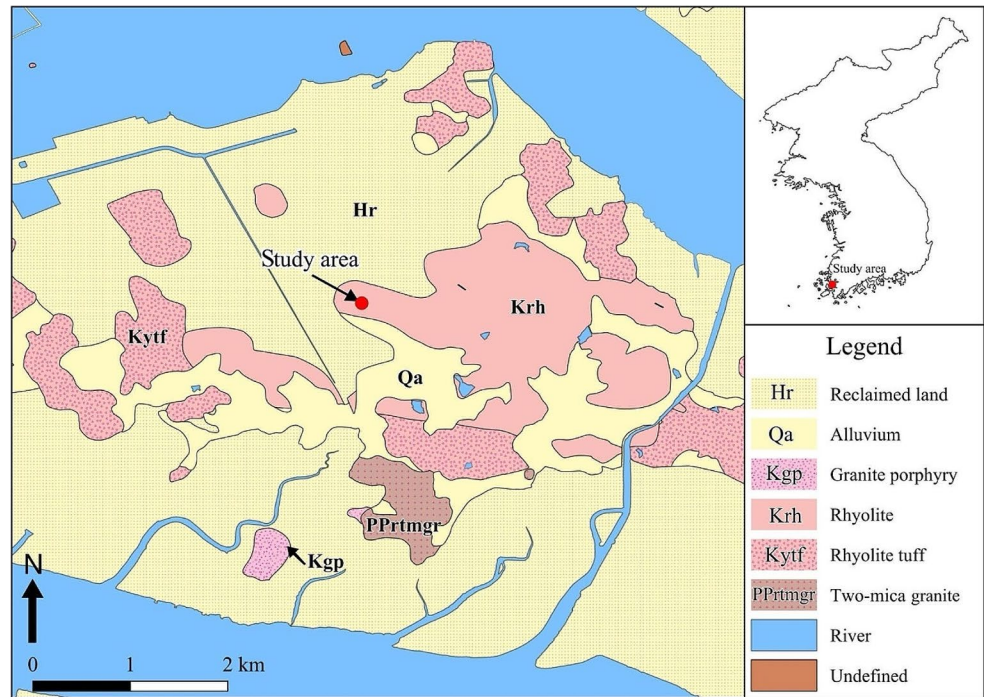

Fig. 14 Proportions of the four joint patterns (total: 2509) in the Yeongam area

and grain boundary fractures (Cuss 1998; Ghasemi et al. 2020; Kranz 1983). Intragranular fractures occur within a single grain, typically due to localized stresses that exceeded the strength of the mineral. Intergranular fractures propagate along a grain boundary rather than through a grain. Intergranular fractures usually occur when the phase in the grain boundary is weak and brittle. In contrast, transgranular fractures travel through several grains of the material. Grain boundary fractures change direction from grain to grain because of the different orientations of the crystal lattices. In other words, when the crack reaches a new grain, it may need to find a new path or plane of atoms to travel on, as it is easier to change the direction of the crack rather than simply continue on the existing propagation path. Cracks tend to follow the paths of least resistance.

Fig. 15 Proportions of the four joint patterns at different depths in the Yeongam area
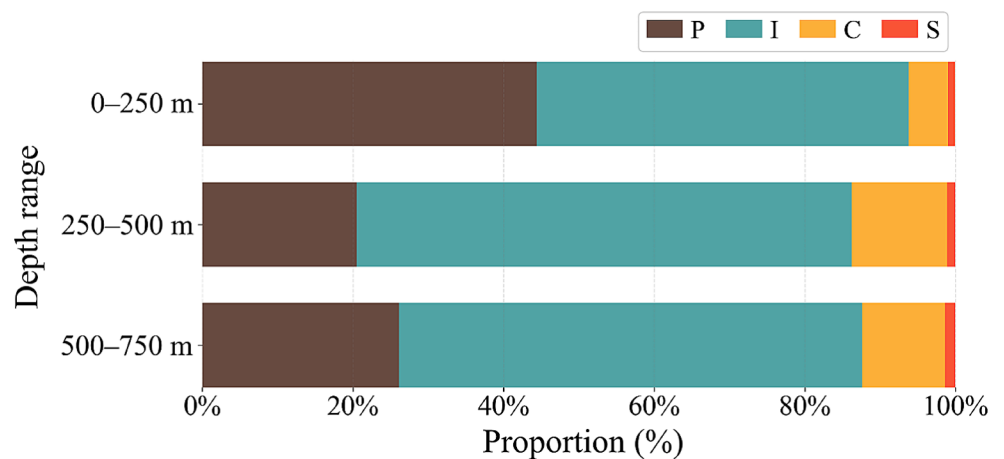
The type of fracture is influenced by the surrounding environment, including factors such as mineral composition, crystal structure, and the presence of grain boundaries. In the case of the porphyroblastic gneiss, the grain boundaries are probably unusually rough because the porphyroblasts are set in a finer-grained matrix. This creates favorable conditions for the generation of I type patterns by boundary cracks. The C type is unusually abundant in rocks of the non-gneissic group, particularly the pegmatites, where they make up 40% of the total fractures. The transition from a ductile to a brittle fracture occurs because of several factors, of which temperature is key. Generally, at higher temperatures, the yield strength decreases, leading to a more ductile fracture. Conversely, at lower temperatures, the yield strength increases, resulting in a more brittle fracture. Considering the mechanism of formation of a pegmatite, which requires high temperatures and encompasses melts, the rock would have become more ductile. This would have allowed for the development of more curved or sinuous joint patterns, which contrasts with more brittle behavior, which would have resulted in planar or stepped joints.

The proposed model for fault zones enabled all faults in the study area to be classified. Although there were two faults exhibiting a complex configuration of types 2 and 4, their chronological order could be established using geological observations. If type 4 had formed after type 2, fault gouges and breccia would not be observed, as they would have undergone lithification. Conversely, in the opposite case, fault gouge and breccia would be discernible. In general, it is known that permeability decreases in a fault core and increases in the damage zone. The geometry and intensity of fracturing of these two elements result in heterogeneity and anisotropy of the overall bulk permeability.

By analyzing the distribution of fault zone patterns by depth, it was observed that the abundance of types 1 and 3 increased with depth whereas types 2 and 4 decreased. This indicates that type 2 is less likely to be generated beyond a depth of 500 m, consequently leading to a reduced number of type 4. It can be assumed that types 1 and 3 require less energy than the other types. Given that fault gouge and breccia could be indicators of fault magnitude, it can be interpreted that the energy involved in forming type 1, with only a fault plane, would be less than that of types 2 and 4, which include gouge and breccia. The relationship between lithology and fault zone patterns was also explored. However, unlike the situation with joint patterns, no strong relationship was identified.

Although the model may not directly provide a numerical value for the hydraulic transmissivity of a fault, it can offer insights into the permeability of the fault zone. According to research on fault zone hydrology (Bense et al. 2013; Caine et al. 1996; Morrow et al. 1981, 1984; Rawling et al. 2001),

the permeability of a fault core is indicated by its thickness, whereas the permeability of the damage zone is indicated by fracture density. It can be inferred that type 2 exhibits high permeability because of its high fracture density near the fault core. Conversely, type 3 would have a lower permeability than type 1, given that its fault core is thicker due to the presence of fault gouge.

To validate the model, the joints in the Yeongam area were classified using the joint model. All joints were successfully classified, proving the validity of the model. The overall distribution of types and the distribution with depth were different in the two study areas, probably because of the different rock types. Volcanic rocks are found mainly in the Yeongam area, and the distribution of P type joints is higher in the Yeongam area than in the Hongcheon area due to the higher proportion of tuff with sedimentary-like bedding. This suggests that the shape of the joint surface is influenced by the mineral composition and internal structure of each rock type. Few faults were found in the Yeongam area, so the fault model will need to be verified in future studies when drillcore data from other areas become available.

The proposed model allows one to estimate the energy of the fault, which influences the spatial arrangement of nearby fractures. The damage index map also indicates that the impact of a fault is reduced at depths beyond ~700 m. Thus, it can be inferred that rock quality is good at depths below 750 m. This aligns with the results concerning the average distances from the fault core of the 10th, 15th, and 20th fractures in directions both toward the surface and downward. As an appropriate depth for geological HLW disposal is crucial for stable isolation, these findings can be used to determine the optimal disposal depth, considering rock stability in relation to faults.

Recent studies have measured the roughness in drillcore using a computer program (Al-Fahmi et al. 2021; Zou et al. 2023). However, these methods are limited in their applicability if conventional well logs are unavailable due to borehole instability. In addition, measuring the JRC of all joints in drillcore is time-consuming whether using contact or non-contact methods. Therefore, the generic model proposed here could be used to analyze joint roughness efficiently while enhancing the accuracy of flow model predictions. In the case of faults, and because faults are known to exhibit scale dependence (Peacock 1996), the use of the fault outcrop model for drillcore has limitations. Given that the model for categorizing faults is usually based on surface observation, the model of this study can be used to characterize the site for geological disposal.

Overall, these simplistic classification models offer the benefit of being efficient and quick methods of characterizing fractures, and they can be applied without being restricted by technical and/or budgetary limitations. A comprehensive

classification model can be built by estimating empirical values of the hydromechanical properties of each joint and fault zone type through further experiments, and assuming representative values for each type of rock. The model can be used to characterize fractures efficiently, particularly in the context of geological disposal site characterization.

Conclusions

In the Hongcheon area, South Korea, 4075 joints and 34 faults were analyzed using a new generic classification model and an earlier proposed model, and both models showed joints and faults fall into four types, based on their geometric characteristics. The classification of joints resulted in the division of joints into planar, irregular, curved, and stepped types, following the earlier conceptual classification of Yoshida et al. (1989) and Du et al. (2014). In the case of faults, fault zones were grouped into type 1 (fault plane without fault gouge), type 2 (the development of fault breccia around fault gouge), type 3 (fault plane with fault gouge), and type 4 (fault plane with lithification). The distribution of joint patterns in the study area was analyzed after examining both the total distribution and depth-specific patterns of the joints along with the distributions of lithologies for each joint pattern. For fault zone patterns, the total distribution, depth-specific distributions, and spatial arrangements near fault cores were investigated using the damage index. The proposed models enabled all the joints and faults to be classified successfully.

Joints can be classified as a planar (P) type if the roughness was low, irregular (I) type if the roughness is high, curved (C) type if the roundness is large, and stepped (S) type if the roundness is small. The study area exhibits a dominance of I types, followed by P, S, and C types. Regarding the distribution of joint patterns by depth, the abundance of I types increased with depth, while the abundance of P and S types decreased. The C type showed no variations with depth. The distribution of joint patterns according to lithology revealed that the I type was relatively abundant in porphyroblastic gneiss, probably because grain boundaries were rougher due to the presence of large porphyroblasts in a fine-grained matrix. This roughness provided favorable conditions for the development of grain boundary fractures, thus leading to I type joints. The C type joints were more abundant in non-gneissic rocks, and particularly in migmatite, and this was probably because the migmatite represents a more ductile rock that was formed under higher temperatures and pressures.

In the case of fault zone patterns, type 2 is most prevalent in the study area, followed by types 1, 3, and 4. The abundance of types 2 and 4 decreased with increasing depth, whereas the abundance of types 1 and 3 increased. This can be related to the fact that an increased load hinders the generation of type 2 as it requires more energy than types 1 and 3. This naturally resulted in a decreasing number of type 4 with increasing depth. The spatial arrangement of fractures near fault cores indicates a decrease in fracture density with increasing depth, both fractures that extend towards the surface and downward. The rock quality tends to improve downward, as is evident on the damage index map.

Earlier research on joints and faults indicated their scale-dependence, and models for their classification are therefore difficult to apply to surface outcrops. However, such models can be applied when drillcores are available, which means they can be used to characterize sites for geological disposal, as disposal typically involves bore-hole drilling. These models offer advantages because they can be used efficiently and speedily to determine the classification parameters that can be used to determine the hydromechanical properties of joints and faults. Lastly, it is necessary to conduct further laboratory tests on the hydraulic conductivity indicated by these models, and to elucidate the influence of mineral composition on crack propagation.

Declarations

References

Al-Fahmi MM, Ozkaya SI, Cartwright JA (2021) FracRough—Computer program to calculate fracture roughness from reservoir rock core. Appl Comput Geosci 9:100045. https://doi.org/10.1016/j.acags.2020.100045

Aydan O, Shimizu Y, Kawamoto T (1996) The anisotropy of surface morphology characteristics of rock discontinuities. Rock Mech Rock Eng 29:47–59. https://doi.org/10.1007/bf01019939

Aydin A (2000) Fractures, faults, and hydrocarbon entrapment, migration and flow. Mar Pet Geol 17:797–814. https://doi.org/10.1016/s0264-8172(00)00020-9

Babanouri N, Nasab SK, Sarafrazi S (2013) A hybrid particle swarm optimization and multi-layer perceptron algorithm for bivariate fractal analysis of rock fractures roughness. Int J Rock Mech Min Sci 60:66–74. https://doi.org/10.1016/j.ijrmms.2012.12.028

Bandis SC, Lumsden AC, Barton NR (1983) Fundamentals of rock joint deformation. Int J Rock Mech Min Sci 20:249–268. https://doi.org/10.1016/0148-9062(83)90595-8

Barton NR (1972) A model study of rock joint deformation. Int J Rock Mech 9:579–602. https://doi.org/10.1016/0148-9062(72)90010-1

Barton NR (1973) Review of a new shear-strength criterion for rock joints. Eng Geol 7:287–332. https://doi.org/10.1016/0013-7952(73)90013-6

Barton NR (1974) Review of a new shear strength criterion for rock joints. Int J Rock Mech Min Sci 11:A220. https://doi.org/10.1016/0148-9062(74)90491-4

Barton NR (1976) The shear strength of rock and rock joints. Int J Rock Mech Min Sci 13:255–279. https://doi.org/10.1016/0148-9062(76)90003-6

Barton NR (1978) Suggested methods for the quantitative description of discontinuities in rock masses: International Society for Rock mechanics. Int J Rock Mech Min Sci 15:319–368

Barton NR (1982) Shear strength investigations for surface mining. In Proceedings of 23rd US Rock Mechanics Symposium. pp 178–180

Barton NR, Choubey V (1977) The shear strength of rock joints in theory and practice. Rock Mech 10:1–54. https://doi.org/10.1007/bf01261801

Barton NR, Quadros E (2015) Anisotropy is everywhere, to see, to measure, and to Model. Rock Mech Rock Eng 48:1323–1339. https://doi.org/10.1007/s00603-014-0632-7

Bense VF, Gleeson T, Loveless SE, Bour O, Scibek J (2013) Fault Zone hydrogeology. Earth Sci Rev 127:171–192. https://doi.org/10.1016/j.earscirev.2013.09.008

Bieniawski ZT (1974) Estimating the strength of rock materials. J South Afr Inst Min Metall 74:312–320. https://doi.org/10.10520/aja0038223x_382

Bodin J, Delay F, de Marsily G (2003) Solute transport in a single fracture with negligible matrix permeability: 2. Mathematical formalism. Hydrogeol J 11:434–454. https://doi.org/10.1007/s10040-003-0269-1

Boutt DF, Grasselli G, Fredrich JT et al (2006) Trapping zones: the effect of fracture roughness on the directional anisotropy of fluid flow and colloid transport in a single fracture. Geophys Res Lett 33:21. https://doi.org/10.1029/2006gl027275

Brown SR (1995) Simple mathematical model of a rough fracture. J Geophys Res 100:5941–5952. https://doi.org/10.1029/94jb03262

Brown SR, Scholz CH (1985) Broad bandwidth study of the topography of natural rock surfaces. J Geophys Res 90:12575–12582. https://doi.org/10.1029/jb090ib14p12575

Caine JS, Evans JP, Forster CB (1996) Fault Zone architecture and permeability structure. Geology 24(11):1025–1028. https://doi.org/10.1130/0091-7613(1996)024%3C1025:fzaaps%3E2.3.co;2

Cardenas MB, Slottke DT, Ketcham RA, Sharp JM Jr (2007) Navier-Stokes flow and transport simulations using real fractures shows heavy tailing due to eddies. Geophys Res Lett 34:L14404. https://doi.org/10.1029/2007gl030545

Cuss RJ (1998) An experimental investigation of the mechanical Behaviour of sandstones with reference to Borehole Stability. University of Manchester, Ph.D.

De Vargas T, Boff FE, Belladona R et al (2022) Influence of geological discontinuities on the groundwater flow of the Serra Geral Fractured Aquifer System. Groundw Sustainable Dev 18:100780. https://doi.org/10.1016/j.gsd.2022.100780

Deb D, Das KC (2010) Extended finite element method for the analysis of discontinuities in rock masses. Geotech Geol Eng 28:643–659. https://doi.org/10.1007/s10706-010-9323-7

Develi K, Babadagli TT, Comlekci C (2001) A new computer-controlled surface-scanning device for measurement of fracture surface roughness. Comput Geosci 27:265–277. https://doi.org/10.1016/s0098-3004(00)00083-2

Du S, Hu Y, Hu X (2009) Measurement of joint roughness coefficient by using profilograph and roughness ruler. J Earth Sci 20:890–896. https://doi.org/10.1007/s12583-009-0075-3

Du S, Hu Y, Hu X (2014) Generalized models for rock joint surface shapes. ScientificWorld J 2014:171873. https://doi.org/10.1155/2014/171873

Fardin N, Stephansson O, Jing L (2001) The scale dependence of rock joint surface roughness. Int J Rock Mech Min Sci 38:659–669. https://doi.org/10.1016/s1365-1609(01)00028-4

Fardin N, Feng Q, Stephansson O (2004) Application of a new in situ 3D laser scanner to study the scale effect on the rock joint surface roughness. Int J Rock Mech Min Sci 41:329–335

Fecker E, Rengers N (1971) Measurement of large scale roughness of rock planes by means of profilograph and geological compass. In: Proceedings Symposium on Rock Fracture, Nancy, France, pp 1–18

Feng Q, Fardin N, Jing L, Stephansson O (2003) A new method for in-situ non-contact roughness measurement of large rock fracture surfaces. Rock Mech Rock Eng 36:3–25

Flodin EA, Aydin A, Durlofsky LJ, Yeten B (2001) Representation of fault zone permeability in reservoir flow models. In: Society of Petroleum Engineers Annual Technical Conference and Exhibition, New Orleans. SPE–71617–MS

Ge Y, Kulatilake PHSW, Tang H, Xiong C (2014) Investigation of natural rock joint roughness. Comput Geotech 55:290–305. https://doi.org/10.1016/j.compgeo.2013.09.015

Ghasemi S, Khamehchiyan M, Taheri A et al (2020) Crack evolution in damage stress thresholds in different minerals of granite rock. Rock Mech Rock Eng 53:1163–1178. https://doi.org/10.1007/s00603-019-01964-9

Grasselli G, Wirth J, Egger P (2002) Quantitative three-dimensional description of a rough surface and parameter evolution with shearing. Int J Rock Mech Min Sci 39:789–800. https://doi.org/10.1016/s1365-1609(02)00070-9

Gudmundsson A (2011) Rock fractures in geological processes. Cambridge University Press, Cambridge, England

Hong ES, Lee JS, Lee IM (2008) Underestimation of roughness in rough rock joints. Int J Numer Anal Methods Geomech 32:1385–1403. https://doi.org/10.1002/nag.678

Hsiung SM, Ghosh A, Ahola MP, Chowdhury AH (1993) Assessment of conventional methodologies for joint roughness coefficient determination. Int J Rock Mech Min Sci Geomech Abstr 30:825–829. https://doi.org/10.1016/0148-9062(93)90030-h

Islam MS, Manzocchi T (2019) A novel flow-based geometrical upscaling method to represent three-dimensional complex subseismic fault zone structures into a dynamic reservoir model. Sci Rep 9:5294. https://doi.org/10.1038/s41598-019-41723-y

Jaeger JC (1959) The frictional properties of joints in rocks. Geofis Pura AppL 43:148–158

Jiang Y, Li B, Tanabashi Y (2006) Estimating the relation between surface roughness and mechanical properties of rock joints. Int J Rock Mech Min Sci 43:837–846. https://doi.org/10.1016/j.ijrmms.2005.11.013

Jiang Q, Feng X, Hatzor YH et al (2014) Mechanical anisotropy of columnar jointed basalts: an example from the Baihetan hydropower station. China Eng Geol 175:35–45. https://doi.org/10.1016/j.enggeo.2014.03.019

Johns RA, Steude JS, Castanier LM, Roberts PV (1993) Nondestructive measurements of fracture aperture in crystalline rock cores using X ray computed tomography. J Geophys Res 98:1889–1900. https://doi.org/10.1029/92jb02298

Keller K, Bonner BP (1985) Automatic, digital system for profiling rough surfaces. Rev Sci Instrum 56:330–331. https://doi.org/10.1063/1.1138299

Kim H, Cho JW, Song I, Min KB (2012) Anisotropy of elasticmoduli, P-wave velocities, and thermal conductivities of Asan Gneiss, Boryeong Shale, and Yeoncheon Schist in Korea. Korea Eng Geol 147:68–77

Kodikara JK, Johnston IW (1994) Shear behaviour of irregular triangular rock - concrete joints. Int J Rock Mech Min Sci 31:313–322

Kranz RL (1983) Microcracks in rocks: a review. Tectonophysics 100:449–480. https://doi.org/10.1016/0040-1951(83)90198-1

Kulatilake PHSW, Shou G, Huang TH, Morgan RM (1995) New peak shear strength criteria for anisotropic rock joints. Int J Rock Mech Min Sci 32:673–697. https://doi.org/10.1016/0148-9062(95)00022-9

Kulatilake PHSW, Balasingam P, Park J, Morgan R (2006) Natural rock joint roughness quantification through fractal techniques. Geotech Geol Eng 24:1181–1202. https://doi.org/10.1007/s10706-005-1219-6

Lee YH, Carr JR, Barr DJ, Haas CJ (1990) The fractal dimension as a measure of the roughness of rock discontinuity profiles. Int J Rock Mech Min Sci 27:453–464. https://doi.org/10.1016/0148-9062(90)90998-h

Lee SH, Lee KK, Yeo IW (2014) Assessment of the validity of Stokes and Reynolds equations for fluid flow through a rough-walled fracture with flow imaging. Geophys Res Lett 41:4578–4585. https://doi.org/10.1002/2014gl060481

Lee HP, Olson JE, Holder J et al (2015) The interaction of propagating opening mode fractures with preexisting discontinuities in shale. J Geophys Res B: Solid Earth 120:169–181. https://doi.org/10.1002/2014jb011358

Li Y, Huang R (2015) Relationship between joint roughness coefficient and fractal dimension of rock fracture surfaces. Int J Rock Mech Min Sci 75:15–22. https://doi.org/10.1016/j.ijrmms.2015.01.007

Li B, Jiang Y, Mizokami T et al (2014) Anisotropic shear behavior of closely jointed rock masses. Int J Rock Mech Min Sci 71:258–271. https://doi.org/10.1016/j.ijrmms.2014.07.013

Liu C, Prévost JH, Sukumar N (2019) Modeling branched and intersecting faults in reservoir-geomechanics models with the extended finite element method. Int J Numer Anal Methods Geomech 43:2075–2089. https://doi.org/10.1002/nag.2949

Lofi J, Pezard P, Loggia D et al (2012) Geological discontinuities, main flow path and chemical alteration in a marly hill prone to slope instability: Assessment from petrophysical measurements and borehole image analysis. Hydrol Process 26:2071–2084. https://doi.org/10.1002/hyp.7997

Maerz NH, Franklin JA, Bennett CP (1990) Joint roughness measurement using shadow profilometry. Int J Rock Mech Min Sci 27:329–343. https://doi.org/10.1016/0148-9062(90)92708-m

Martin V, Jaffré J, Roberts JE (2005) Modeling fractures and barriers as interfaces for flow in porous media. SIAM J Sci Comput 26:1667–1691. https://doi.org/10.1137/s1064827503429363

Menéndez B, Zhu W, Wong TF (1996) Micromechanics of brittle faulting and cataclastic flow in Berea sandstone. J Struct Geol 18:1–16. https://doi.org/10.1016/0191-8141(95)00076-P

Morrow C, Shi LQ, Byerlee J (1981) Permeability and strength of San Andreas Fault gouge under high pressure. Geophys Res Lett 8:325–328. https://doi.org/10.1029/gl008i004p00325

Morrow CA, Shi LQ, Byerlee JD (1984) Permeability of fault gouge under confining pressure and shear stress. J Geophys Res 89:3193–3200. https://doi.org/10.1029/jb089ib05p03193

Patton FD (1966) Multiple modes of shear failure in rock. In: Proceedings of the 1st ISRM Congress. International Society of Rock Mechanics and Rock engineering (ISRM). Lisbon. pp 509–513

Peacock DCP (1996) Field examples of variations in fault patterns at different scales. Terra Nova 8:361–371. https://doi.org/10.1111/j.1365-3121.1996.tb00569.x

Peacock DCP (2001) The temporal relationship between joints and faults. J Struct Geol 23:329–341. https://doi.org/10.1016/S0191-8141(00)00099-7

Petit JP (1987) Criteria for the sense of movement on fault surfaces in brittle rocks. J Struct Geol 9:597–608. https://doi.org/10.1016/0191-8141(87)90145-3

Pirzada MA, Bahaaddini M, Andersen MS, Roshan H (2022) Coupled hydro-mechanical behaviour of rock joints during normal and shear loading. Rock Mech Rock Eng. https://doi.org/10.1007/s00603-022-03106-0

Pollard D, Aydin A (1988) Progress in understanding jointing over the past century. Geol Soc Am Bull 100:1181–1204. https://doi.org/10.1130/0016-7606(1988)100%3C1181:PIUJOT%3E2.3.CO;2

Rasouli V, Harrison JP (2000) Scale effect, anisotropy and directionality of discontinuity surface roughness. In: Proceeding of EUROCK national symposium for Felsmechanik und Tunnelbau, Aacheon. 14:751–756

Rawling GC, Goodwin LB, Wilson JL (2001) Internal architecture, permeability structure, and hydrologic significance of contrasting fault-zone types. Geology 29:43. https://doi.org/10.1130/0091-7613(2001)029%3C0043:iapsah%3E2.0.co;2

Scesi L, Gattinoni P (2007) Roughness control on hydraulic conductivity in fractured rocks. Hydrogeol J 15:201–211. https://doi.org/10.1007/s10040-006-0076-6

Schmittbuhl J, Schmitt F, Scholz C (1995) Scaling invariance of crack surfaces. J Geophys Res 100:5953–5973. https://doi.org/10.1029/94jb02885

Scholtès LUC, Donzé FV (2012) Modelling progressive failure in fractured rock masses using a 3D discrete element method. Int J Rock Mech Min Sci (1997) 52:18–30. https://doi.org/10.1016/j.ijrmms.2012.02.009

Shirono T, Kulatilake PHSW (1997) Accuracy of the spectral method in estimating fractal/spectral parameters for self-affine roughness profiles. Int J Rock Mech Min Sci 34:789–804. https://doi.org/10.1016/s1365-1609(96)00068-x

Son CM, Kim YK, Kim SW, Kim HS (1975) Geological report of the Hongcheon sheet (1:50,000). https://doi.org/10.22747/data.20211022.4503

Sun B, Yang S (2019) An improved 3D finite difference model for simulation of double shield TBM tunnelling in heavily jointed rock masses: the DXL tunnel case. Rock Mech Rock Eng 52:2481–2488. https://doi.org/10.1007/s00603-018-1730-8

Tatone BSA, Grasselli G (2010) A new 2D discontinuity roughness parameter and its correlation with JRC. Int J Rock Mech Min Sci 47:1391–1400. https://doi.org/10.1016/j.ijrmms.2010.06.006

Wu L, Wang Z, Ma D et al (2022) A continuous damage statistical constitutive model for sandstone and mudstone based on triaxial compression tests. Rock Mech Rock Eng 55:4963–4978. https://doi.org/10.1007/s00603-022-02924-6

Wu L, Ma D, Wang Z et al (2023) A deep CNN-based constitutive model for describing of statics characteristics of rock materials. Eng Fract Mech 279:109054. https://doi.org/10.1016/j.engfracmech.2023.109054

Ye Z, Ghassemi A (2018) Experimental study on injection-induced fracture propagation and coalescence for EGS stimulation. The 43rd workshop on Geothermal Reservoir Engineering. Stanford University, Stanford, California

Ye Z, Ghassemi A, Riley S (2018a) Stimulation Mechanisms in Unconventional Reservoirs. In: Proceedings of the 6th Unconventional Resources Technology Conference, Houston, Texas. Society of Exploration Geophysicists, American Association of Petroleum Geologists, Society of Petroleum Engineers. pp 3072–3080

Ye Z, Sesetty V, Ghassemi A (2018b) Experimental and numerical investigation of shear stimulation and permeability evolution in shales. Soc Petrol Eng. https://doi.org/10.2118/189887-MS

Yoshida H, Ohsawa H, Yanagizawa K, Yamakawa M (1989) Analysis of fracture system in Granitic Rock. J Japan Soc Eng Geol 30:131–142. https://doi.org/10.5110/jjseg.30.131

Zhang G, Karakus M, Tang H et al (2014) A new method estimating the 2D joint roughness coefficient for discontinuity surfaces in rock masses. Int J Rock Mech Min Sci 72:191–198. https://doi.org/10.1016/j.ijrmms.2014.09.009

Zheng B, Qi S, Luo G et al (2021) Characterization of discontinuity surface morphology based on 3D fractal dimension by integrating laser scanning with ArcGIS. Bull Eng Geol Environ 80:2261–2281. https://doi.org/10.1007/s10064-020-02011-6

Zimmerman RW, Bodvarsson GS (1996) Hydraulic conductivity of rock fractures. Transp Porous Media 23:1–30. https://doi.org/10.1007/bf00145263

Zimmerman RW, Al-Yaarubi A, Pain CC, Grattoni CA (2004) Nonlinear regimes of fluid flow in rock fractures. Int J Rock Mech Min Sci 41:384–384

Zou L, Jing L, Cvetkovic V (2015) Roughness decomposition and nonlinear fluid flow in a single rock fracture. Int J Rock Mech Min Sci 75:102–118. https://doi.org/10.1016/j.ijrmms.2015.01.016

Zou C, Li J, Wu Y et al (2023) 2D and 3D evaluation of joint roughness exposed by rock cores. Bull Eng Geol Environ 82:1–27. https://doi.org/10.1007/s10064-023-03325-x